Third-Order Intermodulation in a Micromechanical Thermal Mixer

Robert B. Reichenbach, *Student Member, IEEE*, Maxim Zalalutdinov, Keith L. Aubin, Richard Rand, Brian H. Houston, *Member, IEEE*, Jeevak M. Parpia, and Harold G. Craighead, *Member, IEEE*

***Abstract*—A radio frequency (RF) micromechanical shell-type resonator with a resistive thermal actuator is shown to perform as a highly linear, broadband mixer and a high-quality factor post-translation (intermediate frequency) filter. The resistor is capable of frequency translation of RF carrier signals as high as 1.5 GHz to the intermediate frequency of 12.7 MHz. The thermal actuator allows electrical isolation between the input and output of the mixer-filter, dc bias independent mixing, and provides a 50-Ohm load to match the output of front-end electronics. High linearity is demonstrated in the mixer with a third-order input intercept point of +30 dBm for interferers spaced at a 50-kHz offset from the carrier frequency. A variant of the Duffing oscillator model and finite element modeling are used to analyze the origin of nonlinearities in the micromechanical system. [1503]**

***Index Terms*—Bandpass filter, Duffing oscillator, intermediate frequency, microelectromechanical systems (MEMS), mixer, nonlinear oscillations, radio frequency (RF), thermal mechanical coupling, third-order intermodulation distortion (IM_3).**

I. Introduction

CURRENT research in radio frequency microelectromechanical systems (RF MEMS) is significantly motivated by the idea of implementing various types of signal processing in the mechanical domain as opposed to the purely electrical domain [1]. Such a possibility is enabled by scaling laws that shorten the time of mechanical response and bring the resonant frequency of micron-size mechanical structures into the megahertz or gigahertz range [2]. By converting a radio frequency electrical signal into mechanical motion of microfabricated structures and utilizing their resonant properties, one can implement a very narrow pass-band filter (quality factor, $Q \sim 10000$) [3], frequency generator [4] or parametric amplifier [5].

It was recently demonstrated that scaling down MEMS devices also shortens the temperature response time to nanoseconds, enabling another method for RF signal processing based on thermal and mechanical representations of the signal. Zalalutdinov *et al.* have shown that megahertz-range thermal oscillations, induced by a localized heat source, can be efficiently converted into mechanical motion of a high frequency shell-type MEMS resonator (see Fig. 1) [6]. Assuming capacitive pickup for the final transduction from the mechanical motion to the electrical domain, the total path of the associated signal conversion can be viewed as the following: electrical signal-time variable heat-temperature oscillations-resonator stress modulation-mechanical motion-electrical signal.

Fig. 1. Bisection of the polysilcon shell- type micromechanical resonator.

The thermal representation of the signal offers several inherent advantages. It reduces parasitic cross-talk between input and output signal paths and requires only microwatts of an input signal power to produce detectable mechanical motion. Additionally, signal processing based on intrinsic nonlinearity of the thermal response is possible. The fact that the range of the mechanical motion is proportional to the local temperature increase, ΔT, and hence to the square of the applied RF signal, provides a possibility for a broadband mixer implementation.

The combination of a mixer and filter is the core of a heterodyne receiver and largely determines the performance of the device. The presence of high-order nonlinearities in a mixer's response are almost unavoidable for a diode-type or Gilbert cell and contribute to receiver desensitization, harmonic generation and intermodulation between strong signals that are located outside of the frequency band of interest. In this last case, third-order nonlinearities generate new components at $(2f_1 - f_2)$ that may fall within the communication band, masking or corrupting the desired component [7]. A MEMS-based implementation of a mixer-filter reported in [8] exploits the similar nonlinearity of capacitive actuation to perform multiplication; however it suffers from strong higher order terms, which lead to significant intermodulation distortion (IM_3).

In this study we demonstrate a 30 μm diameter shell-type mechanical resonator with a resistive thermal actuator that is capable of downconverting gigahertz frequency signals to the intermediate frequency of the resonator (12.7 MHz). We establish that the quadratic transduction dependence of our MEMS thermal mixer, can be viewed as ideal, i.e., free from third-order intermodulation effects. Since the thermal actuator is essentially an ohmic resistor with negligible reactance, it can also be designed to exactly match the output impedance of the front-end RF electronics in a very wide frequency range.

Manuscript received January 10, 2005; revised May 12, 2005. This work was supported in part by the Cornell Center for Materials Research (CCMR), a Materials Research Science and Engineering Center of the National Science Foundation (DMR-0079992). This work was performed in part at the Cornell Nano-Scale Science & Technology Facility (a member of the National Nanofabrication Users Network) which is supported by the National Science Foundation under Grant ECS-9731293, its users, Cornell University and Industrial Affiliates. Subject Editor N. R. Aluru.

R. B. Reichenbach, M. Zalalutdinov, K. L. Aubin, R. Rand, J. M. Parpia, and H. G. Craighead are with the Cornell Center for Materials Research, Cornell University, Ithaca, NY 14853 USA (e-mail: rbr9@cornell.edu).

B. H. Houston is with Naval Research Laboratories, Washington, DC 20375 USA.

Digital Object Identifier 10.1109/JMEMS.2005.859080

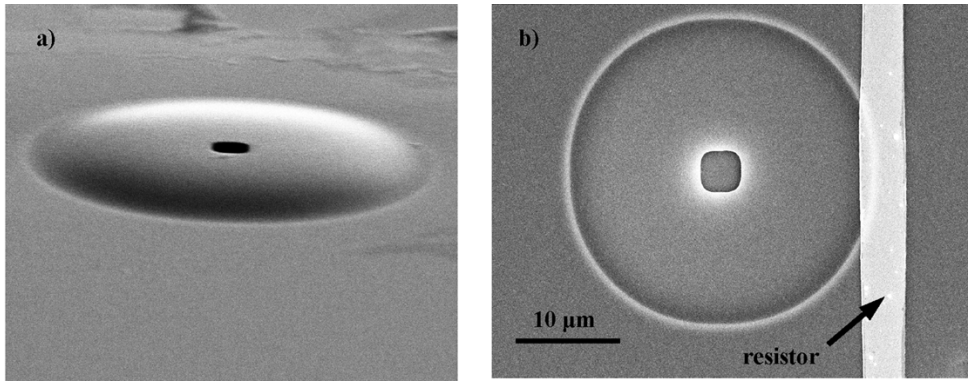

Fig. 2. (a) A 45° SEM of a 30-μm-diameter dome resonator with approximately 1 μm of vertical projection. Dome is fabricated out of 200 nm thick polysilicon over a SiO_2 coated Si wafer. Photolithography and a subsequent RIE etch is used to define the central hole. Hydrofluoric acid removes the underlying SiO_2 through the etch hole which results in a membrane clamped on the periphery and suspended over the substrate in the center. Compressive stress (300 MPa) in the polysilicon film causes out-of-plane buckling in the polysilicon film. (b) Top view of the resonator with a 45 Ω gold resistor defined next to the dome. The white circular ring, which defines the resonator circumference, indicates the edge of the sacrificial oxide below the device layer.

To demonstrate the potential for using MEMS in high performance transceiver applications, we measure the linearity of the MEMS mixer-filter using a two-tone test. The test produces a third-order input intercept point (IIP_3) of $+30$ dBm for interferers spaced at a 50 kHz and 100 kHz offset from the carrier frequency, which is significantly better than the $> +10$ dB specification (10 MHz offset) for 3G W-CDMA [9]. Finally, we develop an analytical model that predicts the behavior of third-order intermodulation in the mechanical resonator initiated by closely spaced interferers, allowing us to predict designs that will reduce the nonlinearity of the resonator.

II. Thermal–Mechanical Transduction

Transduction, the process of producing mechanical motion from a time varying electrical signal, is one of the most significant challenges for micromechanical signal processing devices. Electrostatic actuation, currently the most popular transduction method for MEMS [2], [4], [10] suffers important performance shortcomings. Impedance mismatches between the capacitive actuator and the 50 Ω network either limits the frequency response of the device [8] or causes signal loss. Small gaps between the two electrodes, required to produce significant driving forces, present fabrication and yield challenges. Finally, high dc biases, sometimes on the order of 100's of volts [11], render the method of actuation incompatible with low supply voltage processes.

Thermal–mechanical actuation has been shown to alleviate many of the limitations of electrostatic transduction by replacing the electrostatic driving force with a thermally generated force. Thermal–mechanical transduction relies on a heat source such as a laser [12] or a resistor [3] to produce localized thermal variations on the order of 1 K, which in turn generate detectable mechanical displacement in a thin-film resonator. In the case of the resistor, a thin-film metal microresistor is lithographically defined on the periphery of a dome shaped micromechanical resonator (see Fig. 2). Joule heat dissipated in the microresistor in response to an applied electrical signal changes the local stress field in the polysilicon film. Due to the shallow curvature of the suspended membrane, the stress variations produce vertical displacement in the dome (see Fig. 3).

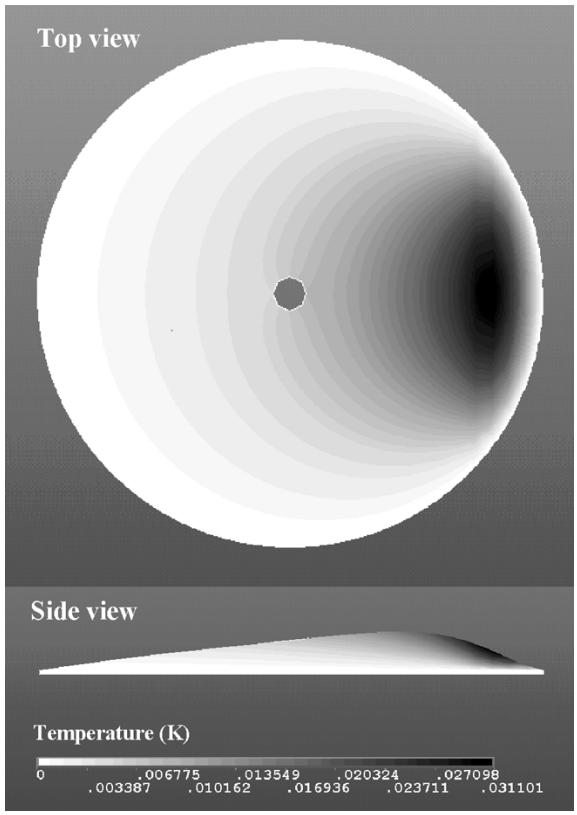

Fig. 3. FEM simulation of temperature variations and static displacement induced by applying a thermal flux of 10 μW dissipated in a 3-μm-wide strip on the polysilicon shell resonator. The periphery of the shell is constrained to be room temperature. A temperature increase of 0.031 K and dc vertical deflection (not pictured to scale) of 0.006 nm is produced in the membrane. $k = 150$ W/mK, $v = 0.22, E = 165$ GPa, $\rho = 2330$ kg/m^3, and $\alpha = 2.6 \times 10 - 6^{-6}$/K.

The change in vertical relief of the structure is detected by a Fabry–Pérot interferometer [14] formed by the cavity between the resonator plate and the substrate. With this method, the output signal from the photodetector is a representation of the resonator mechanical amplitude. The shallow curvature of the device enables us to ensure that the linear portion of the sinusoidal interferometric reflectance pattern (also the region of deepest modulation) occurs at the unperturbed gap distance

by scanning the detection laser ($\lambda = 633$ nm) across the resonator to optimize for the largest magnitude AC signal. The peak-to-peak range of motion is less than 1% of the $\lambda/2$ reflection pattern period; therefore the photodetector representation of the mechanical motion can be approximated as linear.

The mechanical structure of the dome resonates when the frequency of the ac current flowing through the microheater matches a resonant frequency of the dome. The amplitude of the thermally induced mechanical motion is then expanded by the quality factor, Q, of the dome which varies between 3 000 and 10 000 depending on the mode of vibration. The location of the metal heater can be varied to tune the Q of the membrane and can be used to preferentially excite or damp a given mode of resonance. All experiments were performed in vacuum to reduce losses associated with viscous damping, however operation in air has been achieved with a Q of ~ 100.

The primary method for heat dissipation in the membrane is thermal diffusion between the resonator and the bulk polysilicon film [13]. The small thermal time constants of the thin film resonator (less than 1 μs for a 30 μm diameter resonator) allow the incident heat to be modulated and dissipated at a rate comparable to the time constant of mechanical motion at resonance.

At the fundamental frequency (f_o), the force from the resistive actuator driving the mechanical resonator can be expressed as

$$F_{\omega_o} \propto \Delta T \propto V_{\rm dc} V_o \sin(\omega_o t) \tag{1}$$

where V_o is the amplitude of the driving signal at (f_o), $V_{\rm dc}$ is the dc bias on the driving signal, and ΔT is the local change in temperature. Equation (1) is demonstrated experimentally in Fig. 4 where the relative S_{21} S-parameter (the magnitude of the photodetector output signal, divided by V_o from the network analyzer) is plotted versus V_o. For low ac amplitudes, Fig. 4 shows the expected dependence of the resonator amplitude on the dc bias of the driving signal, illustrating how dc bias can be used to control the gain of the MEMS system. S_{21} is seen to be constant for low ac amplitudes until the output no longer follows the input and compression sets in due to nonlinearities. For high dc biases, compression is seen at lower RF drive amplitudes due to higher ac$*$dc drive forces. Thus, a wider input dynamic range can be obtained at lower dc biases, indicating the tradeoff between dynamic range and insertion loss.

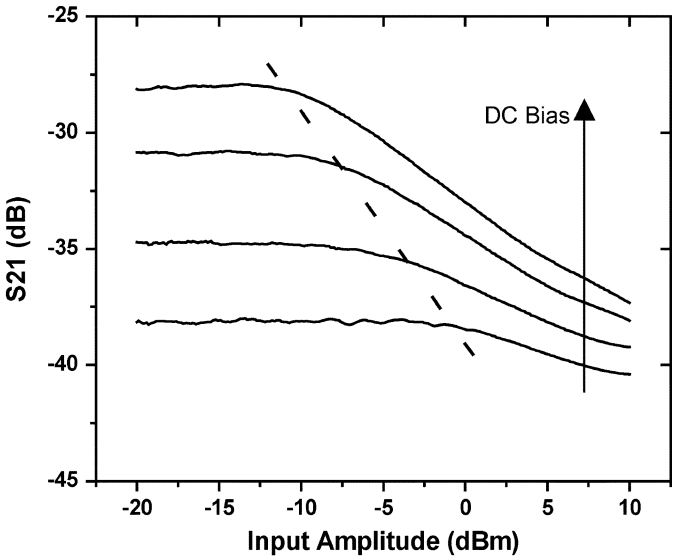

Fig. 4. S_{21} S-parameter (which includes the efficiency of the photodetector and detection optics) of the thermal actuator + resonator sampled at the maximum amplitude of the 12.7 MHz resonant mode. DC bias on the network analyzer drive signal is (from lowest to highest) 75 mV, 100 mV, 150 mV, and 200 mV. Dashed line represents constant mechanical amplitude of 2.5 mV from the photodetector.

III. Thermal Mixing

When two voltage signals are linearly superimposed upon the microheater, the resistor inherently acts as a signal multiplier, analogous to a RF mixer in a heterodyne receiver (Fig. 5b). The driving signal, $V_{\rm RF}$, to the resistor can be represented as the sum of two sinusoids:

$$V_{\rm RF} = V_{\rm dc} + V_1 \sin(\omega_1 t) + V_2 \sin(\omega_2 t). \tag{2}$$

In response to the driving signal, the resistor dissipates power according to V^2/R, where R is the impedance of the microresistor. Since the metal strip is in direct thermal contact with the microresonator film, the local temperature around the strip is directly proportional to the power dissipated by the resistor. We may say that temperature and thus the driving force follow the square of the voltage

$$F_{\rm MIX} \propto \Delta T \propto V_{\rm RF}^2/R = \left(V_{\rm dc} + V_1 \sin(\omega_1 t) + V_2 \sin(\omega_2 t)\right)^2/R. \tag{3}$$

Expanding (3) reveals, among others terms, sum and difference driving frequency components at, $\omega_1 \pm \omega_2$.

$$F_{\rm MIX} \propto V_1 V_2 \cos[(\omega_1 \pm \omega_2)t]/R \tag{4}$$

If the frequencies of the applied signals are chosen such that $f_1 - f_2$ matches the fundamental frequency (f_o) of the dome then appreciable mechanical motion can be observed. This enables the combinatory component to be detected through the amplitude of the mechanical vibrations while other frequency terms in the expansion, which satisfy $1/f \ll \tau_{\rm resonator}$ and $1/f \gg \tau_{\rm resonator}$, are filtered out. In this way, the microheater acts as a frequency converter while the resonator performs intermediate frequency (IF) filtering. Equation (4) illustrates that the driving force provided by the resistive mixer is dc bias independent and thus can produce an IF response in the resonator with no dc voltage on the RF or local oscillator (LO) drive signal.

Fig. 5(a) shows the experimental schematic used to study the micromechanical mixer-filter. Two CW signals from laboratory signal generators are applied to a highly linear power combiner. In the mixer setup, f_1 is the RF carrier frequency (f_c) in the GHz range, and f_2 is the LO frequency, $f_{\rm LO}$, specifically chosen such that $f_c - f_{\rm LO} = f_o$. The subsequent superposition is applied to the microresistor, which heterodynes f_c through the aforementioned process. The now translated RF energy thermally excites a 12.7 MHz resonant mode in the dome resonator and can be detected through the high-Q mechanical passband.

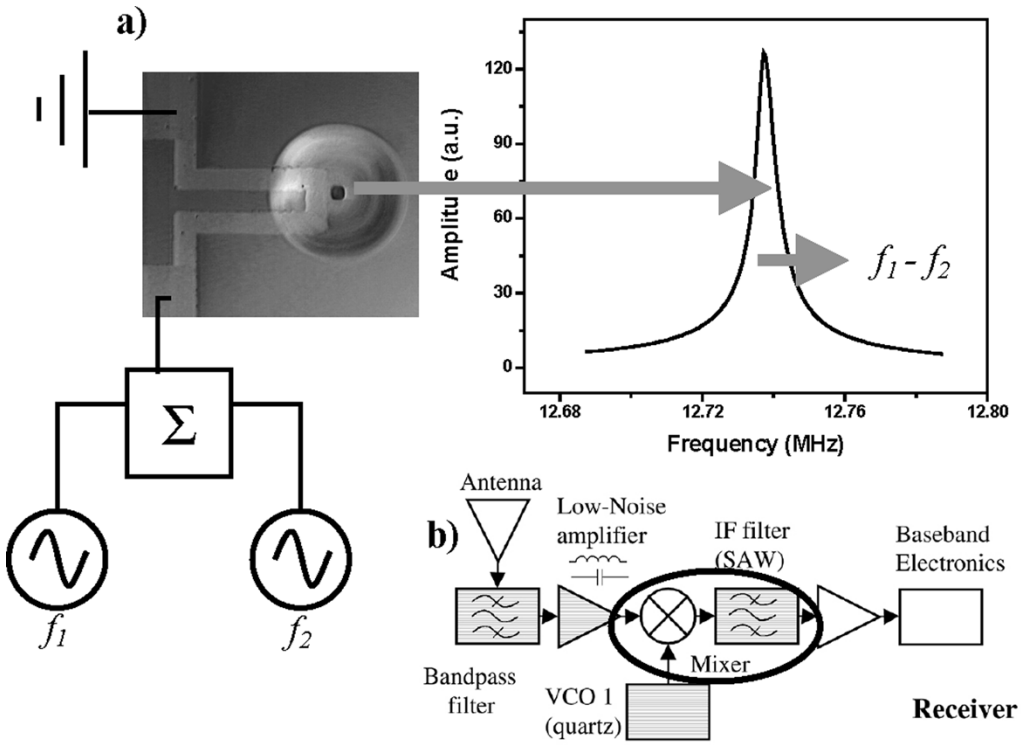

Fig. 5. (a) Diagram of the micromechanical mixer-filter setup where two tones at f_1 and f_2 are applied to the resistor to generate a mechanical response in the resonator at the combinatorial frequency $f_1 - f_2$. (b) Schematic of a heterodyne receiver. Circled area indicates the circuit analogy of the MEMS mixer-filter presented in (a).

IV. RF Input Impedance

An ideal RF mixer has a broadband input frequency response, exhibiting a zero reflection coefficient to any input signal. The frequency dependent input impedance for an electrostatically actuated parallel plate resonator can be derived from the equivalent electrical circuit for the resonator [15]. The expression is minimized at the resonant frequency of the mechanical oscillator; however, the input impedance can be very large for off-resonance driving signals. This presents a problem from two standpoints. First, due to the large out-of-band reflection coefficients, the input frequency range is strictly limited to that of the resonator frequency, eliminating the possibility of down-conversion from a high carrier frequency. Secondly, in order to interface with a RF 50 Ω network, an impedance matching network is needed to transform the high resonator input impedance to that of the input network. This addition causes unwanted power consumption in the low Q passive components and again limits the range of the frequency response of the actuator.

The resistive thermal actuator has the advantage that the dimensions of the resistor can be tailored such that its purely resistive impedance matches that of the input network (50 Ω); a maximum signal transfer match will then occur for any frequency of interest. As a result, input carrier frequencies may encompass a large range, not limited to the bandpass range of an input tuned network or resonator response. The microresistor used in this study (Fig. 2) is configured to be 70 μm × 3 μm × 0.3 μm, which presents a 45 Ω input impedance. Fig. 6 gives the S_{11} reflection coefficient of the thermal actuator. Over a 3 GHz range a nearly constant S_{11} amplitude of -25 dB is maintained, which translates into equal driving magnitudes over the span. For this device we demonstrated an input mixing range up to 1.5 GHz [3]. In our test setup the upper range was limited by parasitic capacitance and inductance associated with the vacuum test chamber and chipset.

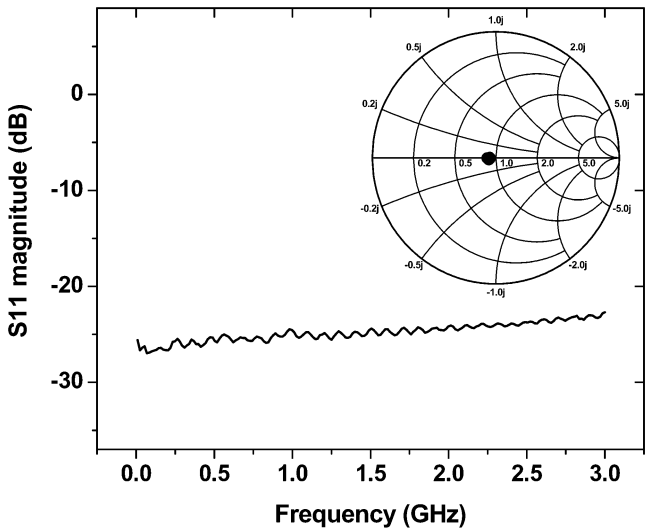

Fig. 6. S_{11} reflection coefficient of the 45 Ω resistive actuator.

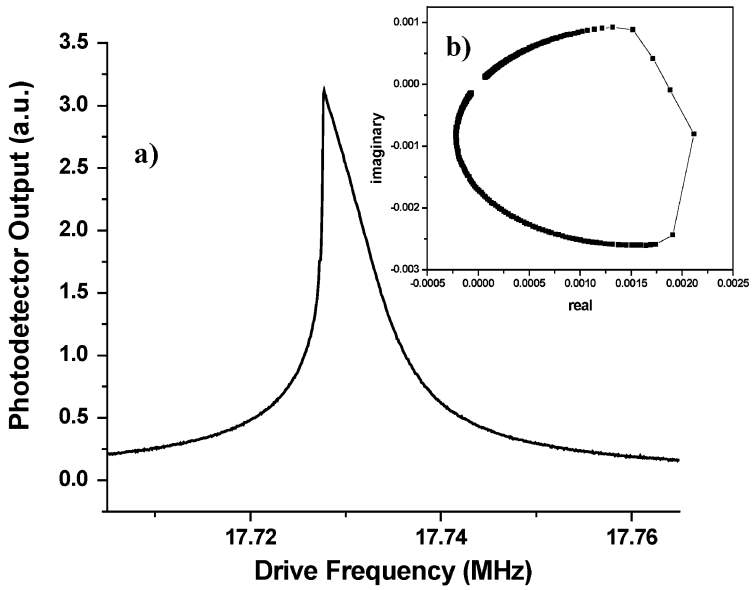

Fig. 7. Nonlinear amplitude response (a) and nyquist plot (b) of a 30-μm resistively driven dome resonator.

V. Nonlinearities

By adopting a "black box" approach, the nonlinearity of an electrical device (or network element) can be expressed in terms of a polynomial dependence

$$U_{\mathrm{OUT}} = \alpha_0 + \alpha_1 U_{\mathrm{IN}} + \alpha_2 U_{\mathrm{IN}}^2 + \alpha_3 U_{\mathrm{IN}}^3 + \ldots \qquad (5)$$

where U_{IN} and U_{OUT} are input and output signals, respectively. RF devices that exhibit a substantial cubic term, α_3, are prone to a phenomenon known as third-order intermodulation (IM_3). When two strong out-of-band interferers are applied to the input of such a device at frequencies $f_1 = f_c + \Delta f$ and $f_2 = f_c + 2\Delta f$, the cubic power component, α_3, will produce a term, U_{IM3}, overlapping with U_{IN}. Substituting $U_{\mathrm{IN}} = U_i(\sin(\omega + \Delta\omega) + \sin(\omega + 2\Delta\omega))$ into (5), we find, among other terms, a third-order term

$$U_{\mathrm{IM3}} = \alpha_3 U_i^3 \sin[(2\omega_1 - \omega_2)t] = \alpha_3 U_i^3 \sin(\omega_c t). \qquad (6)$$

The presence of IM_3 can greatly deteriorate the performance of the device by folding strong out-of-band interferers into the band, which is a primary concern in the design of RF mixers, filters, and amplifiers.

We will show that our thermal mixer can be viewed, in terms of (5), as ideal since its output signal-a temperature, further converted into a force-is an exactly quadratic function of the applied voltage. In other words, for realistic input power ranges, the nonlinearities of the metal-film resistor are negligible. The mechanical filter (the dome resonator) however, can exhibit nonlinear behavior as demonstrated in Fig. 4.

The response of the mechanical resonator to a strong sinusoidal excitation can be calculated using the Duffing equation [16]

$$\frac{d^2x}{dt^2} + \frac{\omega_o}{Q}\frac{dx}{dt} + \left(\omega_o^2 - \beta x^2\right) x = F\sin(\omega t) \qquad (7)$$

which takes into account a nonlinear term β in the resonator spring constant and where x is the displacement around the equilibrium position of the membrane. The presence of β distorts the resonance curve of the dome at large driving amplitudes (see Fig. 7) and thus can produce a significant α_3 term in (5). Since our mixer and filter are inseparable, we must characterize the nonlinearity of the entire device, i.e., mixer-filter combination.

Typically, the magnitude of β is quantified by solving (7) to determine the relationship between the amplitude of oscillation and the deviation from the resonant frequency in the linear regime. However, in the case of MEMS, we do not have an accurate method for determining the absolute amplitude of the mechanical vibrations. To estimate the displacement of the resonator, the modulation of the reflectivity of the built-in Fabry–Pérot interferometer, as a function of the gap, can be calibrated to the mechanical motion by using large displacement MEMS structures [17]. For displacements larger than $\lambda/4$, the reflectance signal will depart from its sinusoidal shape and take on a frequency-doubling characteristic due to movement through interferometric fringes. This allows a fit of the photodetector signal to obtain the value of the mechanical motion. We can use the calibrated laser power (2.25 mW) to measure the modulation of the reflectivity at the apex of the shell resonator and estimate a mechanical amplitude of 1 nm produced by a -10 dBm resistive driving signal.

An alternate method to quantify the severity of nonlinearities, which does not require information about mechanical amplitude, is to analyze effects, such as IM_3, produced by the presence of a third-order term. To quantify IM_3, a special parameter, the third order intercept point (IIP_3), is widely used. IIP_3 is essentially an input power, $\mathrm{P}_{\mathrm{IIP3}}$, that interferers at frequencies f_1 and f_2 would have to impose in order to produce an output signal at a carrier frequency, f_c, that would be as large as the result of applying the same $\mathrm{P}_{\mathrm{IIP3}}$ power input directly at a carrier frequency. In Section IV we will show that IM_3 caused by the resonator can be predicted by solving a modified version of (7).

IM_3 in micromechanical structures has been previously measured for electrostatic force based resonators. Navid *et al.* [18] find an IIP_3 at $\Delta f = 200$ kHz of -3 dBm for a $f_o = 10$ MHz

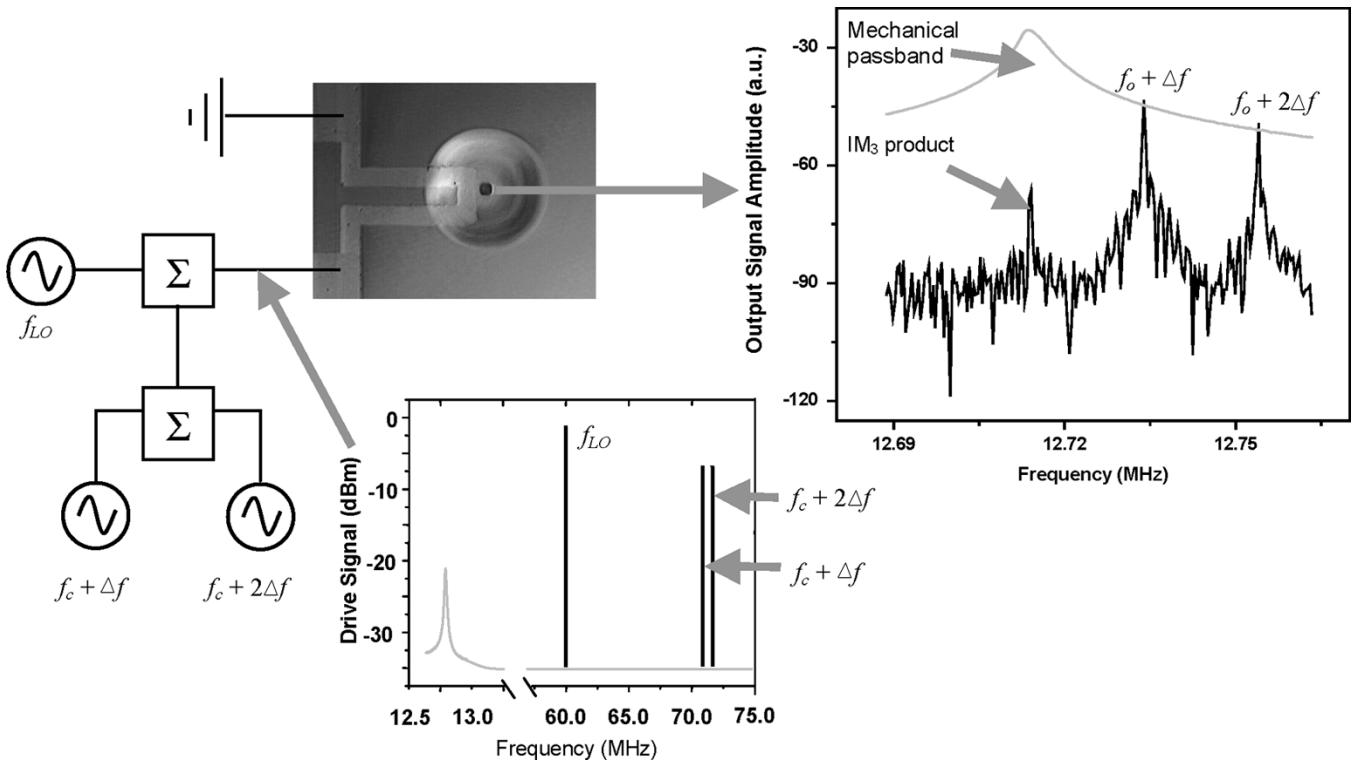

Fig. 8. IM_3 experimental setup for the micromechanical mixer-filter. Two tones, offset from the carrier frequency by Δf and $2\Delta f$, along with a local oscillator signal, are superimposed on the resistor. A third-order intermodulation product at the resonant frequency of the dome, $f_o = 12.7$ MHz is subsequently produced in the mechanical vibrations.

clamped-clamped beam micromechanical resonator implemented as a frequency filter. They find that the electrostatic actuator is the primary source of intermodulation distortion due to the inverse relationship between the parallel plate capacitance and the gap spacing and is limited by the tradeoff between linearity and series motion resistance. To reduce the motional resistance of the capacitive actuator without impacting the linearity of the device, the electrode gaps could be filled with a high-κ dielectric material [19] but this would affect the mechanical quality factor. Kaajakari *et al.* [20] also examine capacitively induced nonlinearities and similarly conclude that, due to distortion in the motional current in an electrostatic MEMS actuator, even linear vibrations can result in harmonic distortion.

Fig. 8 demonstrates the experimental setup for measuring IIP_3 in our MEMS mixer-filter. Three signals (f_{LO}, f_1, and f_2) from external signal sources are linearly superimposed with a power combiner ($\mathrm{IIP}_3 > 50$ dB). The local oscillator (f_{LO}) in the mixer implementation is a 60 MHz, 0 dB signal. The carrier frequency, f_c, in the setup is $f_o + f_{\mathrm{LO}}$, which, for a 12.7 MHz mode in the dome resonator, is chosen to be 72.7 MHz. The test signals (f_1 and f_2) are located at $f_c + \Delta f$ and $f_c + 2\Delta f$, respectively. The signal is then applied to the microheater and IM_3 products are produced at f_o.

Intermodulation was measured at offsets (Δf) between 20 kHz and 500 kHz. Beyond 500 kHz, mechanical attenuation outside the passband of the resonator reduces the magnitude of the interferers and produces very little intermodulation. Fig. 9 plots the output response of the fundamental driving signal, as well as the third-order effects of the two-tone test in relation to the input power. Output power, which is defined by the measurement system, is given in units of dB where the reference level is arbitrary. As expected, the IM_3 strength is greater for in-band interferers than for out-of-band interferers due to the bandpass nature of the mechanical response. A Δf of 20 kHz produced an IIP_3 of $+22$ dBm while a Δf of 200 kHz produced a $+35$ dBm IIP_3.

In order to determine the origin of the nonlinearity, the dome resonators were thermally driven into the nonlinear regime using a 415 nm wavelength modulated diode laser as well as through the electrical resistor. Fig. 10 shows the output response of the dome resonator as a function of the input drive power for the same 12.7 MHz dome resonator mode. A network analyzer directly measures the driving power to the resistor; however, the dissipated power of the laser drive is determined by the gain in the diode laser controller and thus the response can be arbitrarily translated along the horizontal axis in Fig. 10. In general, the laser drive generates larger resonator amplitudes for a given dissipated power because the beam is focused directly on the dome and the position of the laser focus spot is optimized to obtain the largest signal. The resistor is located off the resonator, which minimizes damping due to the metallic film on the resonator but reduces the coupling of the thermal drive. At an output power of -57 dB, the mechanical amplitude produced by both the resistor drive and the laser drive starts to compress, indicating that the onset of nonlinearity is due to large mechanical displacement in the resonator, while higher order nonlinearities in the resistive drive are negligible.

Data from Fig. 4 also suggest that nonlinearities are determined by the resonator by showing that, for a constant V_o, the

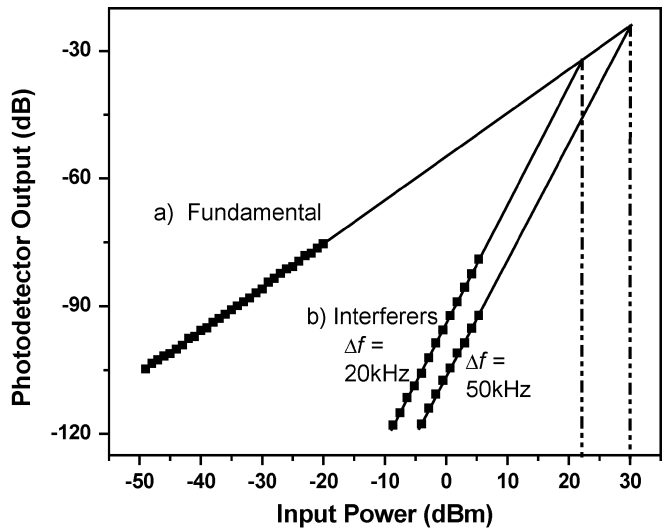

Fig. 9. IM_3 experimental data from the MEMS mixer-filter showing the output response (with an arbitrary reference level) of the resonator at $f_o = 12.7$ MHz in response to a fundamental tone (a) and two off resonance tones spaced from the carrier frequency (72.7 MHz) by $\Delta f = 20$ kHz and 50 kHz (b).

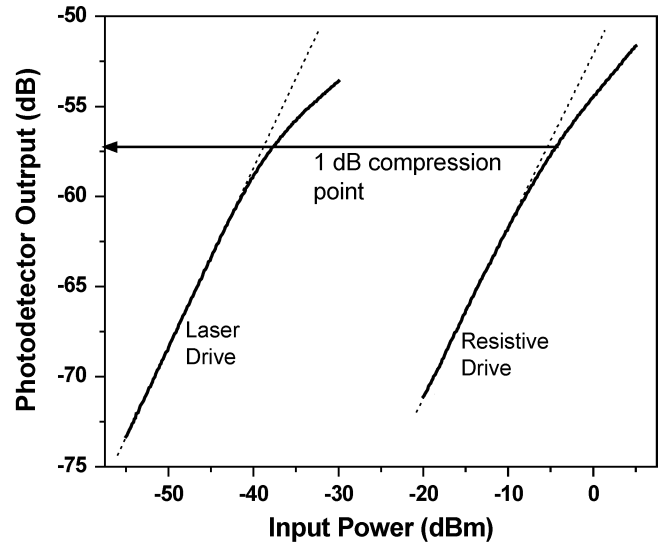

Fig. 10. Curves showing the onset of nonlinearity for a $f_o = 12.7$ MHz resonator in response to a drive signal at f_o (resistor dc bias $= 200$ mV). The 1 dB compression point occurs at a -57 dB output amplitude for both laser thermal drive and resistive thermal drive.

system response may be in either the linear or nonlinear regime, depending on the dc bias. A given V_o that produces a linear response in the resistor + resonator may result in a driving force, $V_o * V_{\mathrm{dc}}$, which generates a nonlinear output signal indicating mechanically determined nonlinearities. In addition, for each dc bias curve in Fig. 4, the 1 dB compression point occurs at the same output amplitude of approximately 2.5 mV from the photodetector as well as at the same $V_o * V_{\mathrm{dc}}$ driving force of ~ 0.25 mW.

For vertical mechanical amplitude of 10 nm at the dome apex (corresponding to 0 dBm resistive drive in Fig. 10) we calculate an in-plane strain of 0.003% in the membrane. This deformation in the resonator is well within the linear elastic regime of the polysilicon film [21] and is unlikely to contribute to nonlinear behavior. Instead, nonlinearities are most likely geometrically

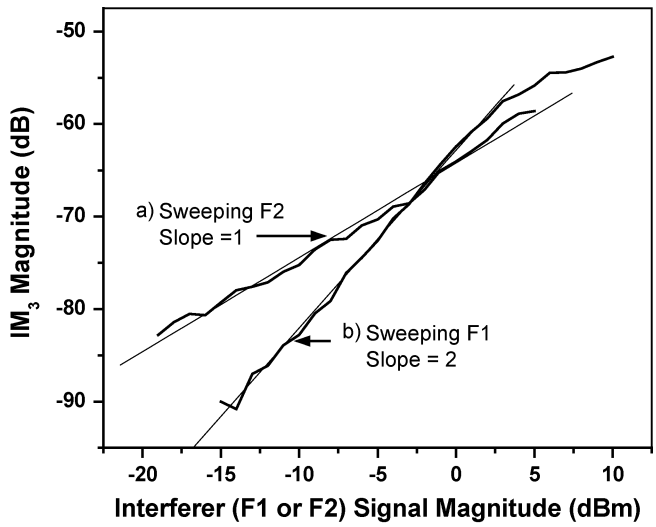

Fig. 11. Magnitude of the resonator amplitude measured at the fundamental frequency, $f_o = 12.7$ MHz, in response to two interferers, where a) the magnitude of F_1 is 0 dBm and the magnitude of F_2 is indicated by the x-axis, and (b) the magnitude of F_2 is 0 dBm and the magnitude of F_1 is indicated by the x-axis.

produced through displacement-induced changes in the spring constant of the resonator.

VI. Analytical Model for Intermodulation

Because the nonlinearities in transduction are due to the mechanical resonator, we seek to understand how the dynamics of the resonator can produce the IM_3 product. We start by modeling the micromechanical filter under out-of-band interferer excitation with a variant of the weakly nonlinear Duffing equation

$$\frac{d^2x}{dt^2} + \varepsilon\frac{\omega_o}{Q}\frac{dx}{dt} + (\omega_o^2 - \varepsilon\beta x^2)x = F_1 \sin\left[(\omega_o + \Delta\omega)t\right] + F_2 \sin\left[(\omega_o + 2\Delta\omega)t\right]. \quad (8)$$

The right hand side of (8) is the forcing function provided by the resistive drive after frequency translation has been performed in the resistor, ε scales damping and nonlinearity as small perturbations to the linear oscillator, and $\beta > 0$ for a softening spring.

Perturbation theory is then applied to (8) in order to gain insight into how the driving terms interact with the βx^3 nonlinear restoring force to produce a response at frequency ω_o. First, we expand the solution to (6) in the form of a power series in ε

$$x(t,\varepsilon) = x_0(t) + \varepsilon x_1(t). \quad (9)$$

Substituting (9) into (8) and grouping terms according to powers of ε, while neglecting terms of order ε^2 and higher, we obtain

$$O(0): \frac{d^2x_0}{dt^2} + \omega_o^2 x_0 = F_1 \sin(\omega_o + \Delta\omega)t + F_2 \sin(\omega_o + 2\Delta\omega)t \quad (10)$$

$$O(1): \frac{d^2x_1}{dt^2} + \omega_o^2 x_1 = -\frac{\omega_o}{Q}\frac{dx_0}{dt} + \beta x_0^3. \quad (11)$$

The solution to (10) is

$$x_0 = R\cos(\omega_o t - \theta) + F_1\frac{\sin(\omega_o + \Delta\omega)t}{\omega_o^2 - (\omega_o + \Delta\omega)^2} + F_2\frac{\sin(\omega_o + 2\Delta\omega)t}{\omega_o^2 - (\omega_o + 2\Delta\omega)^2} \quad (12)$$

where R and θ are constants to be determined. Substituting (12) into (11) results in a myriad of resonant and nonresonant terms. To eliminate secular terms, we set the coefficients of the resonant terms, $\sin(\omega_o t)$ and $\cos(\omega_o t)$, to be zero. Eliminating θ through use of the identity $\sin^2\theta + \cos^2\theta = 1$, we obtain a relation between R, the magnitude of the resonator response at ω_o, and the various parameters. This expression may be simplified by first solving for β and then neglecting all but the lowest order terms in $\Delta\omega$ (since $\Delta\omega$ is assumed to be small compared to ω_o). Solving for R, the expression becomes

$$R = \frac{3\beta F_1^2 F_2 Q}{64\omega_o^5 \Delta\omega^3}. \tag{13}$$

From the approximate solution (13) we see that through third-order nonlinearities present in the mechanical resonator, two appropriately spaced interfering signals will produce an interfering tone on resonance that will grow at a cubic rate, $F_1F_2^2$, when compared to a tone at the fundamental frequency. Equation (13) also implies that intermodulation will substantially decrease as the interfering tones are offset from ω_o, which is experimentally demonstrated in Fig. 9. Finally, R is a decreasing function of the fundamental frequency, indicating that as we move to higher resonator frequencies, the magnitude of the intermodulation will decrease.

To further substantiate (13), we specifically examine the relationship between F_1 and R as well as between F_2 and R. Fig. 11 shows two sets of experimental data from the $\mathbb{IM}_3$ setup measuring the magnitude of the third-order intermodulation at ω_o. In the first set (Fig. 11(a)) the power of the first interferer, $F_1\sin(\omega_o + \Delta\omega)t$, is held constant, while sweeping the power of the second interferer, $F_2\sin(\omega_o + 2\Delta\omega)t$. As expected from (13), Fig. 11 indicates that $\log(R)/\log(F_2) = 1$. The second experiment [see Fig. 11(b)] sweeps the power of the first interferer (F_1) and maintains a constant amplitude second interferer. Again, following (13), $\log(R)/\log(F_1) = 2$.

VII. Conclusion

A micromechanical resonator, thermally actuated by an integrated resistor, is presented for use in RF signal processing circuits. The resistor intrinsically acts as a frequency translation device while the coupled resonator performs postmixing filtering. The input impedance of the actuator can be tuned to match the input network and thus allow wide-band performance. Because overheating in the resistor is less than 1 K, higher order effects in the actuator are shown to be negligible to the point where system nonlinearities are mechanically determined by the resonator. This fact allows very high intermodulation intercept points to be obtained in the micromechanical mixer-filter, even for close band interferers, which is important for reducing off channel interference in RF communications. An analytical model is presented to demonstrate how $\mathbb{IM}_3$ products are produced in the dynamics of a weakly nonlinear micromechanical resonator. The model predicts that, as the natural frequency of the mechanical resonator is increased to higher RF frequencies, $\mathbb{IM}_3$ will be further reduced.

Future work will focus on replacing the He-Ne laser used for interferometric detection with an integrated CMOS amplifier that will measure capacitive displacement currents generated by the resonator. This alteration will allow complete integration into CMOS circuitry and pave the way to a fully integrated RF transceiver (radio-on-chip) with MEMS implementations of all the frequency-determining components.

Acknowledgment

The authors would like to thank Prof. A. Zehnder for discussions related to this paper and Y. Wang for assistance with RF probe measurements.

References

[1] C. T.-C. Nguyen, "Micromechanical devices for wireless communications (invited plenary)," in *Proc. 1998 IEEE International Work Shop on Micro Electro Mechanical Systems*, Heidelberg, Germany, Jan. 25–29, 1998, pp. 1–7.

[2] J. Wang, Z. Ren, and C. T.-C. Nguyen, "Self-aligned 1.14-GHz vibrating radial-mode disk resonators," in *Proc. Dig. Tech. Papers the 12th Int. Conf. on Solid-State Sensors & Actuators (Transducers'03)*, Boston, Massachusetts, Jun. 8–12, 2003, pp. 947–950.

[3] R. B. Reichenbach, M. Zalalutdinov, K. L. Aubin, D. A. Czaplewski, B. Ilic, B. H. Houston, H. G. Craighead, and J. M. Parpia, "Resistively actuated micromechanical dome resonators," in *Proc. SPIE MEMS/MOEMS Components and Their Applications*, San Jose, CA, Jan. 26–27, 2004, pp. 26–27.

[4] V. Kaajakari, T. Mattila, A. Oja, J. Kiihamaki, and H. Seppa, "Square-extensional mode single-crystal silicon micromechanical resonator for low-phase-noise oscillator applications," *IEEE Electron Device Lett.*, vol. 25, no. 4, pp. 173–175, Apr. 2004.

[5] M. Zalalutdinov, A. Zehnder, A. Olkhovets, S. Turner, L. Sekaric, B. Ilic, D. Czaplewski, J. M. Parpia, and H. G. Craighead, "Autoparametric optical drive for micromechanical oscillators," *Appl. Phys. Lett.*, vol. 79, p. 695, 2001.

[6] M. Zalalutdinov, K. L. Aubin, R. B. Reichenbach, A. T. Zehnder, B. Houston, J. M. Parpia, and H. G. Craighead, "Shell-type micromechanical actuator and resonator," *Appl. Phys. Lett.*, vol. 83, pp. 3815–3817, 2003.

[7] B. Razavi, *RF Microelectronics*. Upper Saddle River, NJ: Prentice Hall, 1998.

[8] A.-C. Wong and C.T.-C. Nguyen, "Micromechanical mixer+filters ("mixlers")," *J. Microelectromech. Syst.*, vol. 13, no. 1, pp. 100–112, Feb. 2004.

[9] O. K. Jensen, T. E. Kolding, C. R. Iversen, S. Laursen, R. Reynisson, J. H. Mikkelsen, E. Pedersen, M. B. Jenner, and T. Larsen, "RF receiver requirements for 3G W-CDMA mobile equipment," *Microw. J.*, vol. 43, no. 2, pp. 22–46, 2000.

[10] S. Evoy, D. W. Carr, L. Sekaric, A. Olkhovets, J. M. Parpia, and H. G. Craighead, "Nanofabrication and electrostatic operation of single crystal silicon paddle oscillators," *J. Appl. Phys.*, vol. 86, p. 6072, 1999.

[11] T. Mattila, O. Jaakkola, J. Kiihamaki, J. Karttunen, T. Lamminmaki, P. Rantakari, A. Oja, H. Seppä, H. Kattelus, and I. Tittonen, "14 MHz micromechanical oscillator," *Sens. Actuators A, Phys.*, vol. A97-98, pp. 497–502, Apr. 1, 2002.

[12] M. Zalalutdinov, K. L. Aubin, C. Michael, R. B. Reichenbach, T. Alan, A. T. Zehnder, B. H. Houston, J. M. Parpia, and H. G. Craighead, "Shell-type micromechanical oscillator," in *Proc. SPIE*, vol. 5116, 2003, pp. 229–236.

[13] B. Ilic, S. Krylov, K. Aubin, R. B. Reichenbach, and H. G. Craighead, "Optical excitation of nanoelectromechanical oscillators," *Appl. Phys. Lett.*, vol. 86, p. 193 114, 2005.

[14] D. W. Carr, L. Sekaric, and H. G. Craighead, "Measurement of nanomechanical resonant structures in single-crystal silicon," *J. Vac. Sci. Technol B.*, vol. 16, pp. 3821–3824, Nov./Dec. 1998.

[15] J. Cao and C. T.-C. Nguyen, "Drive amplitude dependence of micromechanical resonator series motional resistance," in *Proc. Dig. Tech. Papers 10th International Conference on Solid-State Sensors and Actuators*, Sendai, Japan, June 7–10, 1999, pp. 1826–1829.

[16] R. H. Rand. (2004) *Lecture Notes on Nonlinear Vibrations* [Online]. Available: http://dspace.library.cornell.edu/handle/1813/79

[17] L. Aubin, M. Zalalutdinov, T. Alan, R. B. Reichenbach, R. Rand, A. Zehnder, J. Parpia, and H. Craighead, "Limit cycle oscillations in CW laser_driven NEMS," *J. Microelectromech. Syst.*, vol. 13, no. 6, pp. 1018–1026, Dec. 2004.

[18] R. Navid, J. R. Clark, M. Demirci, and C. T.-C. Nguyen, "Third-order intermodulation distortion in capacitively-driven CC-beam micromechanical resonators," in *Proc. Tech. Dig. 14 th Int. IEEE Micro Electro Mechanical Systems Conference*, Interlaken, Switzerland, Jan. 21–25, 2001, pp. 228–231.

[19] S. A. Bhave and R. T. Howe, "Internal electrostatic transduction for bulk-mode MEMS resonators," in *Dig. of Tech. Papers the 12th Int. Conf. on Solid-State Sensors & Actuators (Transducers'03)*, Boston, Massachusetts, June 8–12, 2003, pp. 947–950.

[20] V. Kaajakari, T. Mattila, A. Oja, and H. Seppá, "Nonlinear limits for single-crystal silicon microresonators," *J. Microelectromech. Syst*, vol. 13, no. 5, pp. 715–724, Oct. 2004.

[21] W. N. Sharpe Jr, B. Yuan, R. Vaidyanathan, and R. L. Edwards, "Measurements of young's modulus, poisson's ratio, and tensile strength of polysilicon," in *Proc. Tenth Annual International Workshop on Micro Electro Mechanical Systems*, Jan. 26–30, 1997, pp. 424–429.

Robert B. Reichenbach (S'04) received the B.S. degree in engineering and the B.A. degree in economics from Hope College, Holland, MI, in 2001. He is currently pursuing the Ph.D. degree in the Department of Electrical and Computer Engineering at Cornell University, Ithaca, NY.

His research interests include the dynamics of NEMS/MEMS resonators and their applications in RF electronics.

Maxim Zalalutdinov received the Ph.D. degree from the Moscow State University, Moscow, Russia, in 1991.

From 1991 to 1995, he worked with surface analysis and scanning probe microscopy at the Research Institute of Physical Problems, Moscow. From 1995 to 1999, he was with the University of Tokyo, Japan, where his research was related to the physics of quantized vortices in thin superfluid and superconducting films. In 1999, he joined the MEMS group at the Physics Department of Cornell University, Ithaca, NY. His major interest is in nonlinear dynamics of high-frequency MEMS devices.

Keith L. Aubin was born and grew up in Rhode Island. He received the B.S. degree in physics and mathematics in 1998 from the University of Rhode Island, Providence, in 1998. He received the Ph.D. degree from Cornell University, Ithaca, NY.

Presently, he is a Postdoctoral Researcher at Cornell University. Before coming to Cornell University to earn his Ph.D. degree under the direction of Prof. H. Craighead, he worked as an electrical engineer at Cherry Semiconductor, also in Rhode Island. His present research focus is on NEMS/MEMS based biosensors and microfluidic systems.

Richard Rand received the B.S. degree from Cooper Union, NY, in 1964 and the M.S. and Ph.D. degrees from Columbia University, New York, NY, in 1965 and 1967, respectively.

Since 1967, he has been a Professor at the Department of Theoretical and Applied Mechanics, Cornell University, Ithaca, NY. He spent Sabbatical leaves at the Departments of Mechanical Engineering at the University of California, Berkeley, in 1982 and the University of California at Los Angeles (UCLA) in 1989. His current research work involves using perturbation methods and bifurcation theory to obtain approximate solutions to differential equations arising from nonlinear dynamics problems in engineering and biology.

Brian H. Houston (M'02) received B.S., M.S., and Ph.D. degrees in physics from the American University, Washington, DC, in 1980, 1985, and 1989, respectively.

His graduate work concentrated on the polarization dependency of multiphoton ionization of Nobel gasses from metastable energy levels. He joined the Physical Acoustics Branch at NRL in 1980 and built the Experimental Techniques Section (Code 7136). He has developed a broad research program that covers a range of science and engineering disciplines. His personal areas of research include atomic and solid state physics, micro- and nanomechanics, optics, and structural acoustics.

Dr. Houston has received the NRL Alan Berman Research Publication Award five times (1991, 1995, 2000, 2003, and 2005), the NDIA Bronze Medal. He is a Fellow of the Acoustical Society of America.

Jeevak M. Parpia received the B.S. degree in physics from the Illinois Institute of Technology, Chicago, in 1973 and the M.S. and Ph.D. degrees in experimental low temperature physics from Cornell University, Ithaca, NY, in 1977 and 1979, respectively.

In 1979, in became an Assistant Professor at Texas A&M, College Station, and was promoted with tenure in 1984. Since 1986, he has been an Associate Professor and since 1992 a Professor at Cornell's Physics Department. His current research work involves studies of disorder at low temperature on 3He- and glasses, and micromechanical resonators. Hobbies include gardening and historic Indian textiles.

Dr. Parpia was awarded an Alfred P. Sloan Fellowship in 1982 and a Guggenheim Fellowship in 1994 and was elected a fellow of the Americal Physical Society in 2005. From 2000 to 20001 he was a visiting Fellow at the Department of Physics at Royal Holloway College at the University of London.

Harold G. Craighead (M'02) received the B.S. degree in physics (with high honors) from the University of Maryland, College Park, in 1974, and the Ph.D. degree in physics from Cornell University, Ithaca, NY, in 1980. His thesis work involved an experimental study of the optical properties and solar energy applications of metal particle composites.

From 1979 until 1984, he was a Member of Technical Staff at the Device Physics Research Department at Bell Laboratories. In 1984, he joined Bellcore where he formed and managed the Quantum Structures research group. He joined the faculty of Cornell University as a Professor in the School of Applied and Engineering Physics, in 1989. From 1989 until 1995, he was the Director of the National Nanofabrication Facility at Cornell University. From 1998 to 2000, he was the Director of the School of Applied and Engineering Physics and from 2000 to 2001 the founding Director of the Nanobiotechnology Center. He served as Interim Dean of the College of Engineering from 2001 to 2002, after which he returned to the Nanobiotechnology Center as Co-Director for Research. He has been a pioneer in nanofabrication methods and the application of engineered nanosystems for research and device applications. Throughout his career he has contributed to numerous scientific journals with over 270 published papers. He is an inventor on 13 issued patents. His recent research activity includes the use of nanofabricated devices for biological applications. His research continues to involve the study and development of new methods for nanostructure formation, integrated fluidic/optical devices, nanoelectromechanical systems and single molecule analysis.